small methods
www.small-methods.com

In Situ Adjustable Nanogaps and In-Plane Break Junctions

Xueyan Zhao, Xubin Zhang, Kaikai Yin, Surong Zhang, Zhikai Zhao, Min Tan, Xiaona Xu, Zhibin Zhao, Maoning Wang, Bingqian Xu, Takhee Lee, Elke Scheer, and Dong Xiang**

The ability to precisely regulate the size of a nanogap is essential for establishing high-yield molecular junctions, and it is crucial for the control of optical signals in extreme optics. Although remarkable strategies for the fabrication of nanogaps are proposed, wafer-compatible nanogaps with freely adjustable gap sizes are not yet available. Herein, two approaches for constructing in situ adjustable metal gaps are proposed which allow Ångstrom modulation resolution by employing either a lateral expandable piezoelectric sheet or a stretchable membrane. These in situ adjustable nanogaps are further developed into in-plane molecular break junctions, in which the gaps can be repeatedly closed and opened thousands of times with self-assembled molecules. The conductance of the single 1,4-benzenediamine (BDA) and the BDA molecular dimer is successfully determined using the proposed strategy. The measured conductance agreeing well with the data by employing another well-established scanning tunneling microscopy break junction technique provides insight into the formation of molecule dimer via hydrogen bond at single molecule level. The wafer-compatible nanogaps and in-plane dynamical break-junctions provide a potential approach to fabricate highly compacted devices using a single molecule as a building block and supply a promising in-plane technique to address the dynamical properties of single molecules.

1. Introduction

Constructing single-molecule devices not only meets the needs of device miniaturization but also provides a platform to study the intrinsic properties of materials at the single-molecule level.[1–5] Establishing single-molecule junctions is a prerequisite for the realization of functional single-molecule devices.[6–11] Scanning probe microscopy (SPM), such as scanning tunneling microscopy (STM)[12–16] and conducting atomic force microscopy,[17–20] are powerful techniques to generate single-molecule junctions, and many intrinsic properties of single-molecule junctions have been uncovered, promoting the rapid development of molecular electronics. However, the vertically aligned geometry (tip suspended above the substrate) makes SPM facing a great challenge to generate in-plane junctions in which the molecule and two electrodes are aligned in the plane of the same substrate/wafer surface compatible with semiconductor processing technology.[21] Modern micro–nano processing techniques,[22,23] such as electron beam lithography (EBL)[24,25] and focused ion beam,[26,27] show advantages in fabricating scalable on-chip nanogaps down to a few nanometers, providing a potential to realize a highly integrated molecular device. Nevertheless, the size of the gap fabricated directly by these techniques normally cannot be adjusted in situ, which may lead to a low yield of molecular junctions.[28] Mechanically controllable break junctions (MCBJs) technique, in which an electrode pair is fixed on a flexible substrate, can provide precisely controllable gap sizes to match the molecule length, resulting in a high yield of molecular junctions.[29–32] Unfortunately, the three-point bending apparatus only barely allows the control of a few junctions on one chip and also limits its application in compact device manufacturing. In addition, the dynamical bending apparatus hinders its application in the optical research field because the bending of the substrate may require a particular feedback system to keep the light spot focusing on the junction area to eliminate defocusing effect.[33–36]

To meet the requirements of in-plane integration and post-adjustability simultaneously, we present here two straightforward approaches to fabricate adjustable nanogaps based on either a horizontal deformable piezoelectric sheet or a thin stretchable film. Employing a piezoelectric sheet with transverse expansion, the gap size between two metal electrodes can

X. Zhao, X. Zhang, K. Yin, S. Zhang, Z. Zhao, M. Tan, X. Xu, Z. Zhao, M. Wang, D. Xiang
Institute of Modern Optics and Center of Single-Molecule Science
Tianjin Key Laboratory of Micro-scale Optical Information Science and Technology
Nankai University
Tianjin 300350, China
E-mail: xiangdongde@nankai.edu.cn

B. Xu
College of Engineering
University of Georgia
Athens, GA 30602, USA

T. Lee
Department of Physics and Astronomy
and Institute of Applied Physics
Seoul National University
Seoul 08826, Korea

E. Scheer
Department of Physics
University of Konstanz
78457, Konstanz, Germany
E-mail: elke.scheer@uni-konstanz.de

The ORCID identification number(s) for the author(s) of this article can be found under https://doi.org/10.1002/smtd.202201427.

DOI: 10.1002/smtd.202201427

be modulated with atomic resolution in the horizontal direction and a super-large gap size variation up to micrometers can be obtained as well. Employing a stretchable membrane, gold-molecule–gold junctions can be repeatedly formed and separated millions of times. Subsequently, the conductance of a single 1,4-benzenediamine (BDA) molecule and BDA molecular dimer formed via hydrogen bond is statistically determined by employing these in-plane break junction techniques. The measured conductance agrees well with the one determined by the STM break junction (STM-BJ) technique; and thus, confirms the reliability of the proposed in-plane break junction technique.

2. Results and Discussion

2.1. Adjustable Nanogaps Based on Transverse Deformation of Piezo Substrate

Figure 1a schematically shows the fabrication of the adjustable nanogaps based on a piezoelectric ceramic sheet. Here, we take a longitudinal polarized rectangular piezoelectric ceramic sheet[37–40] as the key sandwiched substrate, and the upper and bottom surfaces of the substrate are coated with a silver film as the driving electrodes. A gold wire (100 μm in diameter) with a pre-cut constriction in the middle is fixed on the insulating layer above the top of the silver layer via two drops of glue. The piezoelectric ceramic substrate sandwiched between the two silver electrodes will have a transverse (lateral) deformation when a drive voltage (V_d) is applied to the silver electrodes, whereby the gold wire fixed on the substrate will be stretched by the insulating layer. A signal analyzer is used to monitor the breaking process of the gold wire by measuring the current through the gold wire (Figure S1, Supporting Information). Upon increasing the drive voltage, the tensile stress concentrates at the constriction of the gold wire, triggering a reduction of the cross-section of the constriction until a final break (Figure 1b).

The insert of Figure 1b shows the strain-force distribution as the metal wire is stretched, which is obtained by simulations employing the COMSOL Multiphysics software with the structural mechanics module; see Experimental Section for detailed information.[41] It can be found that the maximum tensile stress (1.35×10^{10} N m^{-2}) is generated around the smallest part of the constriction, which facilitates the break of the gold wire. Obviously, to break the gold wire easily, it is better to make the constriction as narrow as possible. To reduce the diameter of the constriction down to nanometers, a method combining mechanical cutting and electrochemical etching was developed that reduces the diameter of the constriction from micrometers to tens of nanometers; see Figures S2 and S3, Supporting Information, for detailed information.

The ability to control the resolution of the gap size modulation is crucial for the high-yield establishment of molecular devices. We use a 16-bit voltage output module (≈0–10 V) to control the transverse deformation of the piezoelectric ceramics, by which a minimum step of the drive voltage (1 mV) can be realized. This voltage is linearly amplified and applied to the piezoelectric ceramics

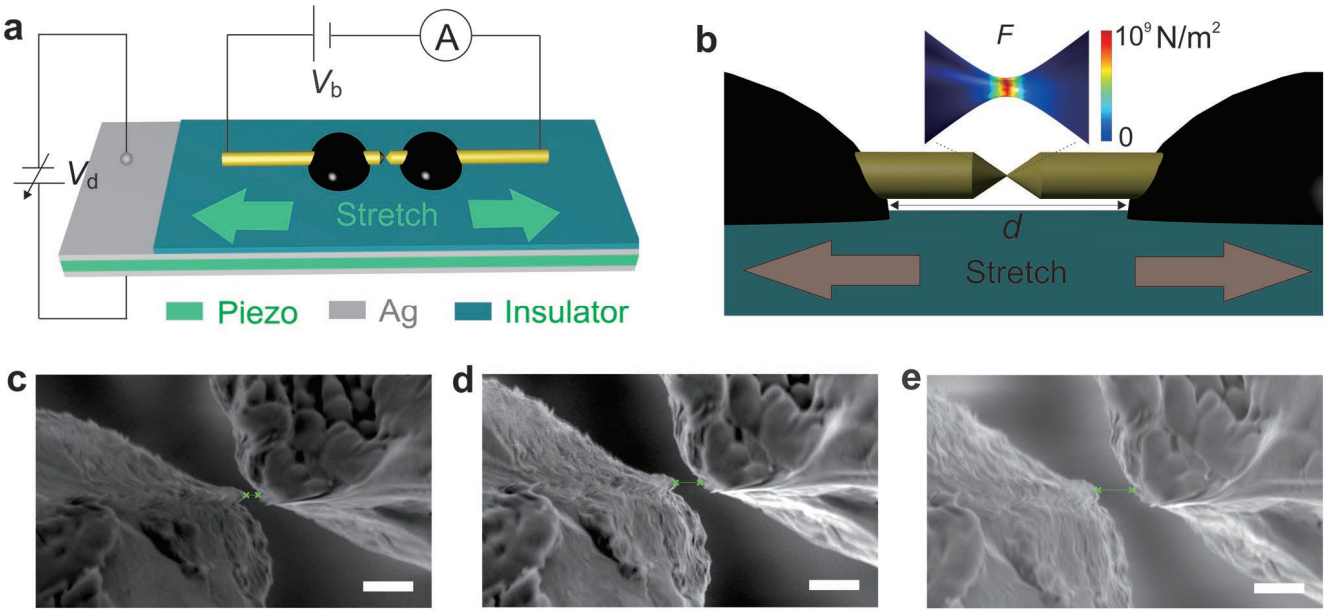

Figure 1. In-plane controllable break junction based on a piezoelectric ceramic sheet. a) Working principle of the in-plane break junction. A longitudinal polarized piezoelectric ceramic sheet is used as the substrate. A transverse deformation will be generated as a drive voltage (V_d) is applied to the substrate, which elongates the gold wire to generate two separated electrodes. The elongation of the gold wire is monitored by applying a bias voltage (V_b) to the gold wire. b) Zoom of the suspended gold wire. The constriction will be elongated until a final break when the underneath substrate undergoes a transverse deformation. The insert shows a simulation of the stress distribution around the constriction when it is stretched. c–e) Scanning electronic microscopy (SEM) images of a gold electrode pair for different drive voltages. A gap size of ≈82, 124, and 232 nm is obtained when a drive voltage of 1, 4, and 10 V is applied to the piezo substrate, respectively. Scale bars: 300 nm for each.

to produce a transverse tensile deformation. The deformation of the piezoelectric sheet is linearly proportional to the applied drive voltage and the maximum transverse deformation is 0.1% of the total length (L) of the piezoelectric sheet upon a maximum drive voltage (V_{max}). Under an applied driven voltage (V_d), the elongation (Δd) of the wire between the two fixed points (d) can be estimated as:

$$\Delta d = (L \times 0.1\%) \times (V_d / V_{max}) \times (d / L) = V_d / V_{max} \times 0.1\% \times d \quad (1)$$

Then, the minimum elongation of the wire can be calculated as:

$$\Delta d_{min} = V_{min} / V_{max} \times 0.1\% \times d = 1\,mV / 10\,V \times 0.1\% \times d = 10^{-7} \times d \quad (2)$$

Accordingly, the maximum elongation of the gold wire can be calculated as:

$$\Delta d_{max} = V_{max} / V_{max} \times 0.1\% \times d = 10^{-3} \times d \quad (3)$$

Based on Equation (2), the minimum step of the separation of the electrodes (Δd_{min}) linearly depends on the initial distance (d) between the two points fixed by glue, which provides an adjustable resolution for the gap size control. To control the gap more precisely, the gold wire can be fixed by two closely separated glue drops (e.g., $d \approx 1$ mm); then, the gap size can be precisely adjusted with sub-nanometer resolution ($\Delta d_{min} = 10^{-7} \times d \approx 10^{-7} \times 1$ mm = 0.1 nm) based on Equation (2). Without special requirement for the gap control, the gold wire can be fixed by two glue drops separated far away (for e.g., $d \approx 10$ mm), enabling adjustment of the gap size with nanometer resolution ($\Delta d_{min} = 10^{-7} \times d \approx 10^{-7} \times 10$ mm = 1 nm) based on Equation (2). Despite the reduced modulation resolution, the gap size can be adjusted to offer a super-large gap size variation ($\Delta d_{max} = 10^{-3} \times d \approx 10$ μm) based on Equation (3) with the coarse-tuning mode. Figure 1c–e shows, with closely separated glue drops, a gap size of ≈82, 124, and 232 nm can be obtained as a driven voltage of 1, 4, and 10 V is output and applied to the sample, respectively. In contrast, with faraway separated glue drops, a gap size of ≈0.4, 2.4, and 5.2 μm is obtained upon the same drive voltages, respectively (Figure S4, Supporting Information).

Thus far, we have demonstrated gluing a notched wire on the substrate can offer a gap size varied from nanometers to micrometers with adjustable modulation resolution. It is known that lithographically defined MCBJs chips have a much smaller footprint than those made of glued wires for the realization of integrated functional devices.[42,43] We further fabricated nanoscale metallic bridge suspended above a piezoelectric ceramic which can be developed into electrode array in principle using lithography technique. Detailed information regarding the fabrication process can be found in Figure S5, Supporting Information. The working principle of this strategy is schematically shown in **Figure 2**a and the SEM image of the fabricated sample is shown in Figure 2b. The zoomed SEM image of the constriction upon different drive voltages is shown in Figure 2c–e. An unstretched nanobridge can be observed when no drive voltage is applied (Figure 2c). The nanobridge break and a gap with a size of ≈25 nm are observed when a drive voltage of 5 V is output and applied to the piezoelectric sheet (Figure 2d). The gap size is enlarged from ≈25 to ≈42 nm when the drive voltage increases from 4 to 10 V. The gap size can be reduced by decreasing the drive voltage. It had been found that the conductance decreases in step with heights in the order of G_0 by continuously increasing the drive voltage, proving that atomic-size contacts can be provided by the in-plane break junction (Figure S6, Supporting Information).

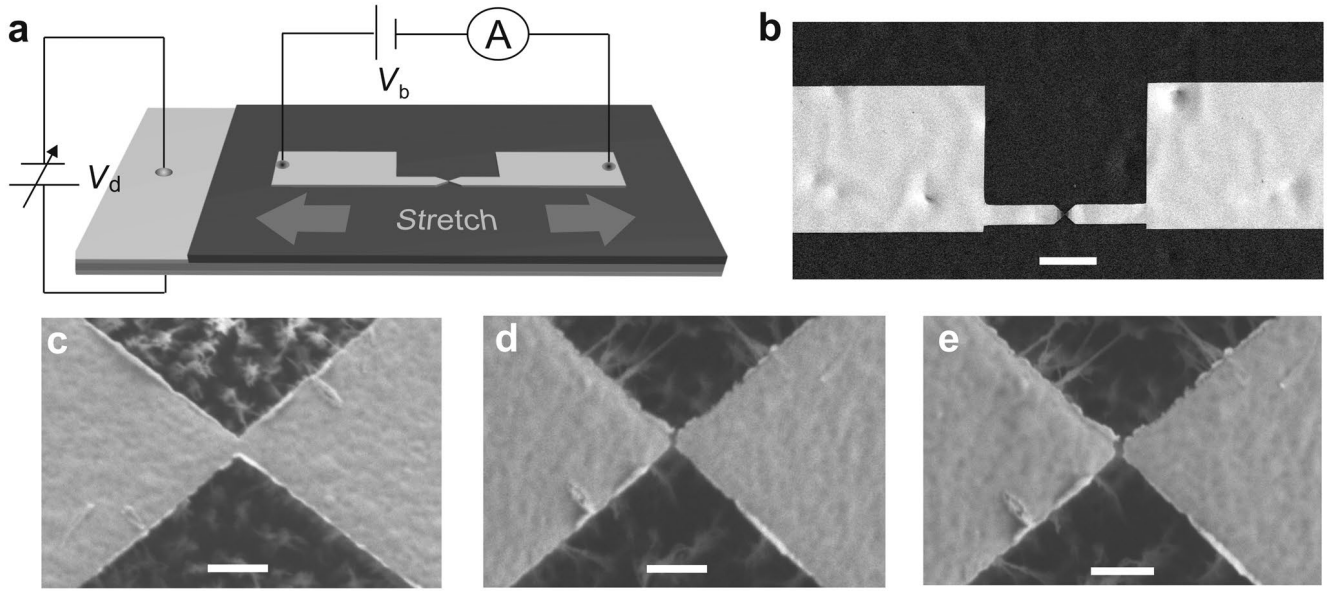

Figure 2. Adjustable nanogaps based on electron beam lithography (EBL). a) Working principle of the adjustable nanogaps based on EBL. b) The SEM image of the sample. Scale bar: 20 μm. c) Close-up of the suspended nanobridge without drive voltage (V_d = 0 V). d) The nanobridge was stretched and a nanogap (≈25 nm) was observed when a drive voltage (V_d = 5 V) was applied to the underneath piezoelectric substrate. e) The nanogap increases to ≈42 nm when a drive voltage V_d = 10 V is applied. Scale bars: 200 nm for (c–e).

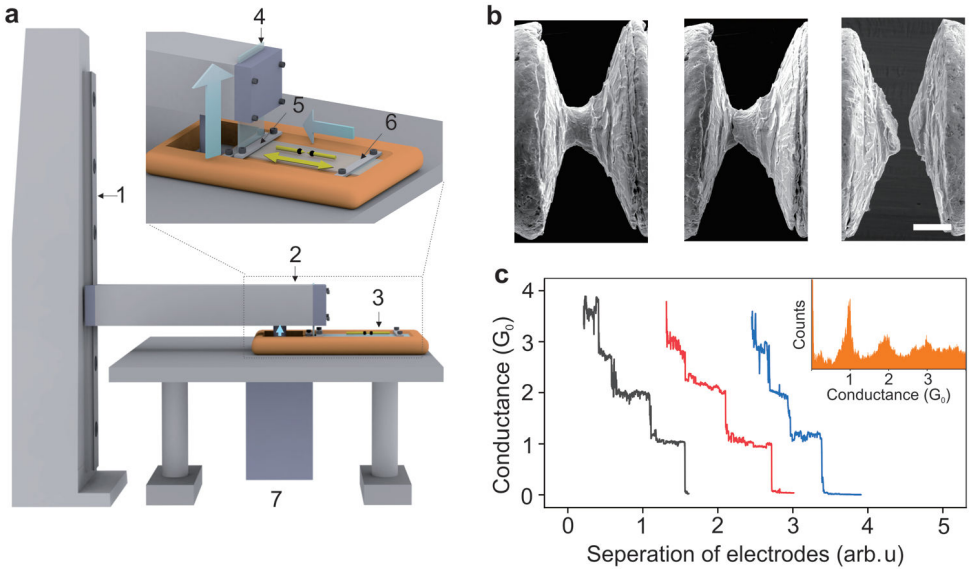

Figure 3. Mechanically controllable in-plane break junctions based on a stretchable membrane. a) Working principle of the in-plane break junctions. The gold wire with a constriction is fixed above a stretchable TPU membrane. The stretching of the membrane will elongate the gold wire until a final break of the gold wire, generating two separated electrodes. The relaxing of the membrane will make the separated electrodes recontact. Insert: the vertical movement of the piezo component causes a horizontal stretching of the membrane via a slot. 1: Slide rail; 2: Cantilever; 3: Gold wire; 4: Flexible film; 5: Slot to steer the membrane from horizontal to vertical direction; 6: Steel sheet to fix one end of the membrane; 7: Piezo component to generate a pushing force to move the cantilever in the vertical direction. b) SEM image of the gold electrodes with a separation controlled by the stretching of the membrane. Scale bar: 20 µm. c) The typical conductance traces of the gold contacts decrease in steps near multiples of G_0 ($= 2e^2/h$) during the breaking process. Insert: 1D conductance histogram constructed from 500 conductance traces as presented in (c) shows well-defined peaks near 1 G_0, 2 G_0, and 3 G_0.

2.2. In-Plane Break Junctions by Stretching a Flexible Membrane

For the strategy proposed above, a disadvantage is that the deformation-driving voltage source is very close to the nanogap (the piezo substrate is just isolated by a thin insulation layer); and thus, the driving electric field may interfere with the electron transport inside the nanogap. To overcome this problem, an alternate approach based on continuously mechanically stretching a flexible membrane is proposed, where the deformation-driving field source is far away from the working electrodes and nano gap. **Figure 3**a shows the working principle of this proposed in-plane break junction that as a proof-of-principle uses again a glued notched wire. Briefly, a gold wire with a constriction is fixed on a stretchable membrane (thermoplastic polyurethane, TPU) with two drops of epoxy resin. One end of the flexible membrane is fixed on the substrate by a steel sheet, and the other end is fixed on a cantilever via a slot to steer the horizontal membrane toward a vertical direction. The cantilever can be pushed to move along the vertical direction by a bar connected to a piezo component. The vertical movement of the cantilever will stretch the membrane in the horizontal direction; and thus, the gold wire fixed by two drops of glue will be gradually elongated until it breaks at the constriction. The gap between the electrodes can be gradually reduced until a recontact when the membrane is gradually relaxed by adjusting the piezo voltage. Similar to the case of the MCBJ method, the separation of the electrodes is attenuated with respect to the displacement of the piezo;[44] the total stretching length of the membrane is equal to the displacement of the piezo but only the small part between the two glue drops causes the separation of the electrodes. The attenuation factor obviously depends on the distance between the glue drops and the membrane size and typically amounts to (10^{-3}–10^{-4}). More detailed information regarding the fabrication of the setup can be found in Figure S7, Supporting Information. The SEM images of the gold constriction during the stretching process are shown in Figure 3b, demonstrating that different gap sizes up to micrometers can be obtained by the controlled stretching and relaxing of the membrane.

To verify the reliability of the proposed in-plane break junctions, we measured the conductance of a bare metal electrode during the breaking process using statistical methods. Figure 3c shows the typical conductance traces of Au—Au contacts with a bias voltage of 100 mV. The conductance typically decreases in a step of G_0 ($= 2e^2/h$). Here, e is the electron charge, and h is Planck's constant. The inset shows the corresponding conductance histograms constructed from 500 conductance traces recorded during the electrode separation process without any data selection. The conductance histogram shows well-defined quantized conductance peaks located near 1 G_0, 2 G_0, and 3 G_0, demonstrating that an atomic scale nanobridge can be fabricated employing this mechanically controllable in-plane break junction technique. The chip can straightforwardly be miniaturized by using EBL-defined bridges as the starting point. It would then allow to operate several tunable junctions on one membrane by proper arrangement of the junctions.[45]

2.3. Conductance of Single-Molecule and Molecular Dimer Junctions

We further apply this in-plane break junction technique by stretching a membrane to measure the single-molecule conductance.[46] 1,4-benzenediamine (BDA) with amino anchor

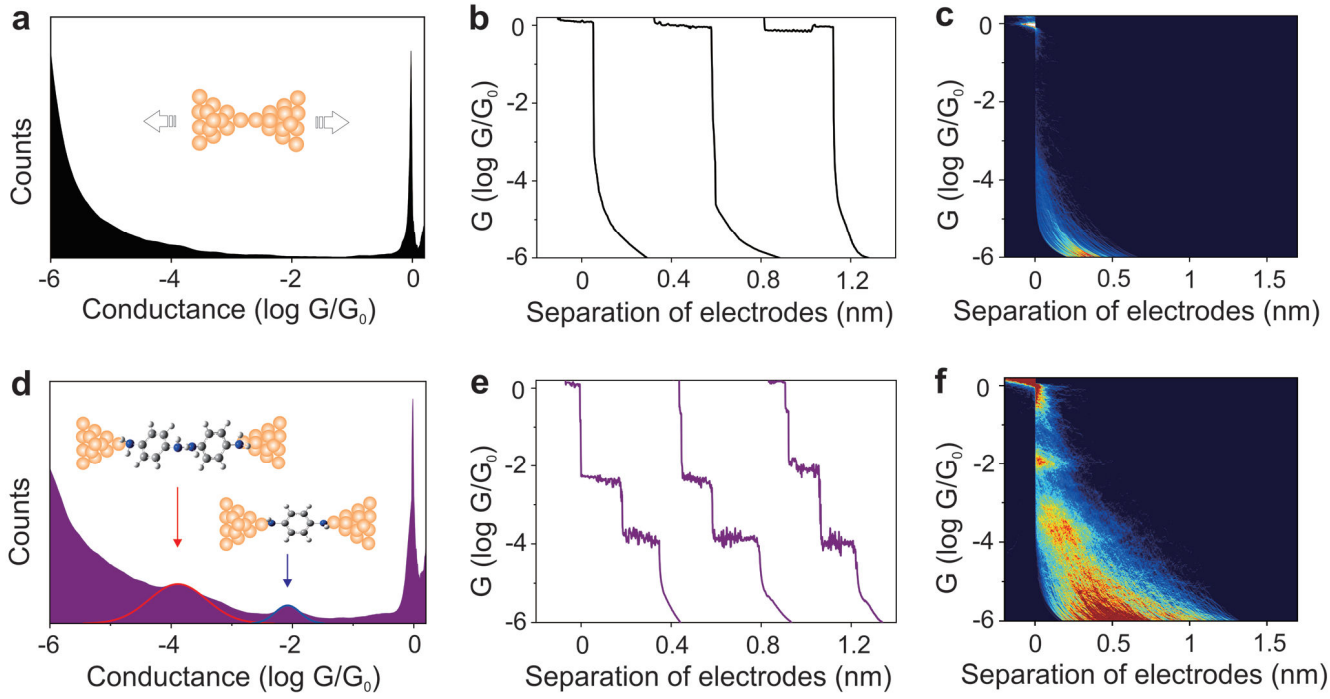

Figure 4. Conductance measurement of single molecule (dimer) junctions. a–c) Characterization of the bare gold wire during the separation. 1D conductance histogram of bare gold wire constructed from 715 conductance traces. Insert: Schematic of the bare atomic junction (a). Typical conductance traces of bare gold junctions recorded during the electrodes separation process (b). The corresponding 2D conductance histogram of bare gold junctions (c). d–f) Characterization of gold junctions after BDA molecule assembling process. 1D conductance histogram of the molecule containing junctions constructed from 1925 conductance traces. Two Gaussian fitting curves (red and blue) determine two probable conductance values ($\approx 7.8 \times 10^{-3}$ G_0 and 1.3×10^{-4} G_0). Insert: Schematic of a single BDA molecular junction and a BDA dimer junction formed via a hydrogen bond (d). Typical conductance traces of the BDA containing junctions recorded during electrodes separation (e). 2D conductance histogram of the BDA molecule containing junctions (f).

groups ($-NH_2$) at two ends was selected as the target molecule. The measurements were performed under ambient conditions immediately after the self-assembling of BDA (≈0.1 mM) in an aqueous solution and drying with nitrogen. The experiment with bare metal electrodes without molecules is used as a blank control. **Figure 4**a shows the 1D conductance histogram constructed from 715 conductance traces without data selection. There is only one pronounced peak near 1 G_0, which can be assigned to the conductance of the gold single-atom contact before the break (insert).[13] Figure 4b shows the typical conductance traces recorded during the separation process of two bare electrodes, showing only one plateau at 1 G_0. Figure 4c shows the corresponding 2D conductance histogram. Both Figure 4b and Figure 4c show that there are no additional plateaus below 1 G_0 for these bare electrode break junctions. In contrast, additional pronounced two peaks near 7.8×10^{-3} G_0 and 1.3×10^{-4} G_0 are observed in the conductance histogram when the experiment is performed after BDA molecules self-assembling on the electrode surface (Figure 4d). In this case, two additional conductance plateaus below 1 G_0 are also observed in the conductance traces (Figure 4e) as well as in the 2D conductance histogram (Figure 4f).

Notably, the membrane between the two fixed points is only stretched/relaxed by a few nanometers for each open/close cycle, and the whole membrane is only stretched/relaxed by a few micrometers. Meanwhile, we choose thermoplastic polyurethane (TPU), known for its excellent mechanical strength and low-temperature elasticity, as flexible membrane. Therefore, obvious fatigue of the membrane in the experiments is not observed at room temperature, even though thousands of opening/closing cycles are performed. Figure S8, Supporting Information, shows two typical opening traces, one recorded at the beginning of an experiment and one after ≈2000 opening/closing cycles. The slope of the conductance traces in the tunneling regime is very similar, suggesting the aging problem in our experiment is trivial.

To confirm the reliability of the proposed in-plane break junction technique, scanning tunneling microscopy break junction (STM-BJ) experiments were further performed and the data obtained by both techniques were compared with each other. The conductance histograms by STM-BJ experiments also showed that there are two pronounced conductance peaks with a high and a low conductance located at $\approx 7.7 \times 10^{-3}$ G_0 and $\approx 1.3 \times 10^{-4}$ G_0 (Figure S9a–e, Supporting Information), which agreed well with the observations presented in Figure 4d,f. The high conductance value ($\approx 7.8 \times 10^{-3}$ G_0) being consistent with previous reports,[47–49] was assigned to the conductance of BDA single-molecule junctions. Notably, the sample was thoroughly rinsed with pure solvent and dried with nitrogen after the self-assembling process in our experiment. Thus, the possibility for π–π stacking between two BDA molecules was very low. The very small peak around 10^{-4} G_0 was statistically not significant.

Both experimental and theoretical studies have shown that a dimer may form between two imidazole molecules through a hydrogen bond.[50,51] Accordingly, we attribute the observed low conductance ($\approx 1.3 \times 10^{-4}$ G_0) to the BDA dimer junction formed

via a hydrogen bond. To further confirm that the low conductance truly results from the BDA dimer, ethanol was added during the self-assembling process which could dissociate the intermolecular hydrogen bond because ethanol can form new hydrogen bonds with BDA; thus, destroying the original hydrogen bonds.[52] It is found that only the high conductance peak is presented, that is, the low conductance peak disappears after adding ethanol (Figure S9d–f, Supporting Information). This observation supports our hypothesis that the low conductance originates from the BDA dimer formed via the intermolecular hydrogen bond. In addition, the conductance of BDA molecular junctions was addressed by employing the mechanically controllable break junction technique, which shows two conductance peaks coherent with the ones by employing our novel on-chip break junction and STM-BJ techniques (see Figure S10, Supporting Information). These STM-BJ and MCBJ experiments not only confirm the reproducibility of the observation but also prove the reliability of the above proposed in-plane break junction technique.

3. Conclusion

To summarize, gapped electrodes with on-chip adjustable gap size are fundamental building blocks for the fabrication of nanometer-sized devices and molecule-based integrated circuits. Here, two types of strategies for fabricating in-plane nanogaps based on the transverse expansion of a piezoelectric sheet or mechanically stretching a flexible membrane are demonstrated for the first time. The fabricated nanogaps not only meet the requirement of on-chip wafer-compatibility but also of flexible adjustability to realize high-yield functional molecular devices. Avoiding chemical etching and EBL process, a straightforward strategy to realize in-plane break junction based on stretching a flexible membrane is further proposed. Moreover, a vivid application is demonstrated in measuring the single-molecule and molecule dimer conductance employing the designed in-plane break junctions. By comparing to the data obtained by the STM-BJ method, the reliability of the proposed in-plane technique to characterize the properties of single molecule junctions is demonstrated. Our results provide insight into the formation of molecule dimer via hydrogen bond at single molecule level. The in-plane nanogaps/junctions provide a promising approach to foster the integration of single molecules as building blocks. The in situ adjustable nanogaps also provide a potential application in extreme optics (for example, tip-enhanced Raman spectroscopy and localized surface plasmons) without defocusing effect.

4. Experimental Section

Single-Molecule Conductance Measurement by STM-BJ: The single-molecule conductance measurements of target molecules were performed using the STM-BJ technique.[53] The gold substrate was prepared by Plasma sputtering 2 nm Cr and 150 nm gold on silicon in an HV chamber, and immersing in 0.5 mM BDA aqueous solution or BDA solution with ethanol solution for 12 h, respectively. They were then thoroughly rinsed with aqueous solution and blown dry with nitrogen. The STM tip was prepared by burning one end of a gold wire (99.999%, 0.25 mm in diameter) with a butane mixture flame to form a ball. The 100 mV bias voltage was applied between two gold electrodes.

Simulation of Force Distribution: The force distribution around the constriction upon stretching was simulated with structural mechanics module employing COMSOL finite element simulation software. The diameter of the initial gold wire was set to 100 μm and the smallest diameter of the constriction was set to 1 μm. The gold wire was fixed on the piezoelectric ceramic substrate, and the length of the suspended part (d) was set to 200 μm. Accordingly, the total stretch length of the nanobridge was set to 200 nm (0.1% of the suspended length), which was possible with the piezoelectric ceramic sheet used in the authors' experiments.

In Situ Observation of the Electrode Stretching: The observation of electrode stretching was performed using the modified Scanning Electron Microscope (SEM, Sigma 500, Zeiss Germany. The original blind flange on the chamber of the SEM was replaced by a customized blind flange with two ceramic sealed electrodes connecting the inside and outside of the chamber. After placing the fabricated chip into the chamber, one end of the electrode (inside the chamber) was connected to the piezoelectric ceramic substrate via vacuum-enameled wires, and the other end of the electrode (outside the chamber) was connected to the voltage output module via an amplifier, which supplied a drive voltage to control the deformation of the piezoelectric substrate via a home-made control software.

Supporting Information

Supporting Information is available from the Wiley Online Library or from the author.

Acknowledgements

X. Zhao and X. Zhang contributed equally to this work. The authors acknowledge the financial support from the National Key R&D Program of China (2021YFA1200103), the National Natural Science Foundation of China (22273041, 91950116, 11804170), and the Natural Science Foundation of Tianjin (19JCZDJC31000, 19JCJQJC60900).

Conflict of Interest

The authors declare no conflict of interest.

Data Availability Statement

The data that support the findings of this study are available in the supplementary material of this article.

Keywords

adjustable nanogaps, hydrogen bond, in-plane break junctions, single molecule study, wafer compatible nanogaps

Received: November 2, 2022
Revised: December 27, 2022
Published online: February 2, 2023

[1] G. E. Moore, *Proc. IEEE* **1998**, *86*, 82.
[2] A. Aviram, M. A. Ratner, *Chem. Phys. Lett.* **1974**, *29*, 277.

[3] A. Vilan, D. Aswal, D. Cahen, *Chem. Rev.* **2017**, *117*, 4248.
[4] V. R. Stamenkovic, D. Strmcnik, P. P. Lopes, N. M. Markovic, *Nat. Mater.* **2017**, *16*, 57.
[5] S. J. van der Molen, R. Naaman, E. Scheer, J. B. Neaton, A. Nitzan, D. Natelson, N. J. Tao, H. S. J. van der Zant, M. Mayor, M. Ruben, M. Reed, M. Calame, *Nat. Nanotechnol.* **2013**, *8*, 622.
[6] J. H. Tian, Y. Yang, B. Liu, B. Schöllhorn, D. Y. Wu, E. Maisonhaute, A. S. Muns, Y. Chen, C. Amatore, N. J. Tao, Z. Q. Tian, *Nanotechnology* **2010**, *21*, 274012.
[7] S. R. Zhang, C. Guo, L. Ni, K. M. Hans, W. Zhang, S. Peng, Z. Zhao, D. C. Guhr, Z. Qi, H. Liu, M. Song, Q. Wang, J. Boneberg, X. Guo, T. Lee, E. Scheer, D. Xiang, *Nano Today* **2021**, *39*, 101226.
[8] Y. Kanamaru, M. Ando, J. Shirakashi, *J. Vac. Sci. Technol., B* **2014**, *33*, 02B106.
[9] L. Cui, Y. Zhu, M. Abbasi, A. Ahmadivand, B. Gerislioglu, P. Nordlander, D. Natelson, *Nano Lett.* **2020**, *20*, 6067.
[10] H. Jeong, H. B. Li, L. Domulevicz, J. Hihath, *Adv. Funct. Mater.* **2020**, *30*, 2000615.
[11] L. J. O'Driscoll, M. R. Bryce, *Nanoscale* **2021**, *13*, 10668.
[12] H. Ohnishi, Y. Kondo, K. Takayanagi, *Nature* **1998**, *395*, 780.
[13] B. Q. Xu, N. J. Tao, *Science* **2003**, *301*, 1221.
[14] Z. Yu, Y. X. Xu, J. Q. Su, P. M. Radjenovic, Y. H. Wang, J. F. Zheng, B. Teng, Y. Shao, X. S. Zhou, J. F. Li, *Angew. Chem., Int. Ed.* **2021**, *60*, 15452.
[15] B. Xiao, S. He, M. Sun, J. Zhou, Z. Wang, Y. Li, S. Liu, W. M. Nau, S. Chang, *Angew. Chem., Int. Ed.* **2022**, *61*, e202203830.
[16] W. Lee, S. Louie, A. M. Evans, N. M. Orchanian, I. B. Stone, B. Zhang, Y. Wei, X. Roy, C. Nuckolls, L. Venkataraman, *Nano Lett.* **2022**, *22*, 4919.
[17] T. W. Kelley, E. Granstrom, C. D. Frisbie, *Adv. Mater.* **1999**, *11*, 261.
[18] M. S. Hybertsen, L. Venkataraman, *Acc. Chem. Res.* **2016**, *49*, 452.
[19] K. Dalla Francesca, S. Lenfant, M. Laurans, F. Volatron, G. Izzet, V. Humblot, C. Methivier, D. Guerin, A. Proust, D. Vuillaume, *Nanoscale* **2019**, *11*, 1863.
[20] Z. Xie, I. Bâldea, Q. V. Nguyen, C. D. Frisbie, *Nanoscale* **2021**, *13*, 16755.
[21] D. Xiang, X. L. Wang, C. C. Jia, T. Lee, X. F. Guo, *Chem. Rev.* **2016**, *116*, 4318.
[22] S. H. Luo, B. H. Hoff, S. A. Maier, J. C. de Mello, *Adv. Sci.* **2021**, *8*, 2102756.
[23] C. Jia, A. Migliore, N. Xin, S. Huang, J. Wang, Q. Yang, S. Wang, H. Chen, D. Wang, B. Feng, Z. Liu, G. Zhang, D.-H. Qu, H. Tian, M. A. Ratner, H. Q. Xu, A. Nitzan, X. Guo, *Science* **2016**, *352*, 1443.
[24] Z. S. Gan, Y. Y. Cao, R. A. Evans, M. Gu, *Nat. Commun.* **2013**, *4*, 2061.
[25] E. Lörtscher, J. W. Ciszek, J. Tour, H. Riel, *Small* **2006**, *2*, 973.
[26] H. Li, I. H. Wani, A. Hayat, S. H. M. Jafri, K. Leifer, *Appl. Phys. Lett.* **2015**, *107*, 103108.
[27] P. Gu, W. Zhang, G. Zhang, *Adv. Mater. Interfaces* **2018**, *5*, 1800648.
[28] T. Li, W. P. Hu, D. B. Zhu, *Adv. Mater.* **2010**, *22*, 286.
[29] C. J. Muller, J. M. van Ruitenbeek, L. J. de Jongh, *Phys. Rev. Lett.* **1992**, *69*, 140.
[30] M. A. Reed, C. Zhou, C. J. Muller, T. P. Burgin, J. M. Tour, *Science* **1997**, *278*, 252.
[31] Z. K. Zhao, C. Guo, L. Ni, X. Zhao, S. Zhang, D. Xiang, *Nanoscale Horiz.* **2021**, *6*, 386.
[32] D. Xiang, H. Jeong, T. Lee, D. Mayer, *Adv. Mater.* **2013**, *25*, 4845.
[33] Z. K. Zhao, R. Liu, D. Mayer, M. Coppola, L. Sun, Y. Kim, C. Wang, L. Ni, X. Chen, M. Wang, Z. Li, T. Lee, D. Xiang, *Small* **2018**, *14*, 1703815.
[34] C. Y. Guo, X. Chen, S. Y. Ding, D. Mayer, Q. Wang, Z. Zhao, L. Ni, H. Liu, T. Lee, B. Xu, D. Xiang, *ACS Nano* **2018**, *12*, 11229.
[35] D. Benner, J. Boneberg, P. Nürnberger, R. Waitz, P. Leiderer, E. Scheer, *Nano Lett.* **2014**, *14*, 5218.
[36] M. Wang, T. Wang, O. S. Ojambati, T. J. Duffin, K. Kang, T. Lee, E. Scheer, D. Xiang, C. A. Nijhuis, *Nat. Rev. Chem.* **2022**, *6*, 681.
[37] J. F. Tressler, S. Alkoy, R. E. Newnham, *J. Electroceram.* **1998**, *2*, 257.
[38] J. Rödel, K. G. Webber, R. Dittmer, W. Jo, M. Kimura, D. Damjanovic, *J. Eur. Ceram. Soc.* **2015**, *35*, 1659.
[39] L. Li, M. H. Wu, *Nano Energy* **2021**, *83*, 105786.
[40] W. K. Lin, B. Wang, G. Peng, Y. Shan, H. Hu, Z. Yang, *Adv. Sci.* **2021**, *8*, 2002817.
[41] J. Wang, C. Gao, X. Duan, K. Mao, *J. Electr. Eng. Technol.* **2015**, *10*, 176.
[42] J. Ruitenbeek, A. Alvarez, I. Pineyro, C. Grahmann, C. Urbina, *Rev. Sci. Instrum.* **1996**, *67*, 108.
[43] C. Zhou, C. J. Muller, M. R. Deshpande, J. W. Sleight, M. A. Reed, *Appl. Phys. Lett.* **1995**, *67*, 1160.
[44] N. Agraït, A. Levy Yeyati, J. M. van Ruitenbeek, *Phys. Rep.* **2003**, *377*, 81.
[45] R. Waitz, O. Schecker, E. Scheer, *Rev. Sci. Instrum.* **2008**, *79*, 093901.
[46] H. Liu, Z. Zhao, X. Zhao, M. Wang, T. Zhao, D. Xiang, *AIP Adv.* **2022**, *12*, 075307.
[47] L. Venkataraman, J. E. Klare, C. Nuckolls, M. S. Hybertsen, M. L. Steigerwald, *Nature* **2006**, *442*, 904.
[48] S. Y. Quek, L. Venkataraman, H. J. Choi, S. G. Louie, M. S. Hybertsen, J. B. Neaton, *Nano Lett.* **2007**, *7*, 3477.
[49] L. Venkataraman, Y. S. Park, A. C. Whalley, C. Nuckolls, M. L. Steigerwald, *Nano Lett.* **2007**, *7*, 502.
[50] Z. Zhao, C. Guo, L. Ni, X. Zhao, D. Xiang, *Nanoscale Horiz.* **2021**, *6*, 386.
[51] H. Chen, J. Fraser Stoddart, *Nat. Rev. Mater.* **2021**, *6*, 804.
[52] L. Ge, S. Hou, Y. Chen, Q. Wu, L. Long, X. Yang, Y. Ji, L. Lin, G. Xue, J. Liu, X. Liu, C. J. Lambert, W. Hong, Y. Zheng, *Chem. Sci.* **2022**, *13*, 9552.
[53] L. Wang, Z. L. Gong, S. Y. Li, W. Hong, Y. W. Zhong, D. Wang, L. J. Wan, *Angew. Chem., Int. Ed.* **2016**, *55*, 12393.